ACS APPLIED MATERIALS & INTERFACES

Research Article

www.acsami.org

Silicon Surface Deoxidation Using Strontium Oxide Deposited with the Pulsed Laser Deposition Technique

Zoran Jovanović,*[,†,§] Matjaž Spreitzer,[†] Janez Kovač,[‡] Dejan Klement,[†] and Danilo Suvorov[†]

[†]Advanced Materials Department and [‡]Department of Surface Engineering and Optoelectronics, Jožef Stefan Institute, Jamova 39, 1000 Ljubljana, Slovenia

[§]Laboratory of Physics, Vinča Institute of Nuclear Sciences, University of Belgrade, P.O. Box 522, 11001 Belgrade, Serbia

ABSTRACT: The epitaxial growth of functional oxides on silicon substrates requires atomically defined surfaces, which are most effectively prepared using Sr-induced deoxidation. The manipulation of metallic Sr is nevertheless very delicate and requires alternative buffer materials. In the present study the applicability of the chemically much more stable SrO in the process of native-oxide removal and silicon-surface stabilization was investigated using the pulsed-laser deposition technique (PLD), while the as-derived surfaces were analyzed *in situ* using reflection high-energy electron diffraction and *ex situ* using X-ray photoelectron spectroscopy, X-ray reflectivity, and atomic force microscopy. After the deposition of the SrO over Si/SiO_2, in a vacuum, different annealing conditions, with the temperature ranging up to 850 °C, were applied. Because the deposition took place in a vacuum, a multilayer composed of SrO, Sr-silicate, modified Si, and Si as a substrate was initially formed. During the subsequent annealing the topmost layer epitaxially orders in the form of islands, while a further increase in the annealing temperature induced rapid desorption and surface deoxidation, leading to a 2 × 1 Sr-reconstructed silicon surface. However, the process is accompanied by distinctive surface roughening, and therefore the experimental conditions must be carefully optimized to minimize the effect. The results of the study revealed, for the first time, an effective pathway for the preparation of a SrO-induced buffer layer on a silicon substrate using PLD, which can be subsequently utilized for the epitaxial growth of functional oxides.

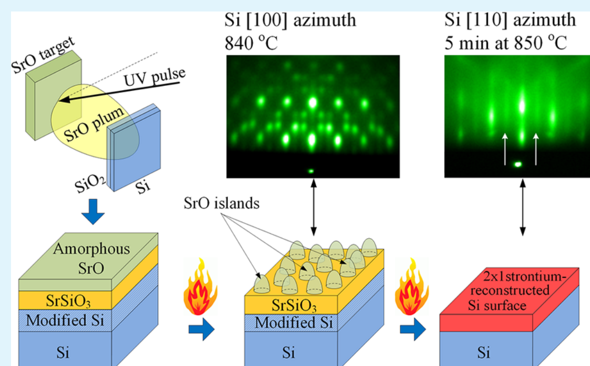

KEYWORDS: *buffer layer, interface reactions, strontium silicate, surface reconstruction, functional oxides*

INTRODUCTION

In recent years there has been an increasing interest in the integration of functional metal oxides with silicon that would expand the possibilities and application of silicon-based technologies. The research is driven by the wide range of properties exhibited by metal oxides, some of which are unique (e.g., metallic conductivity at the interface between two insulating oxides, $LaAlO_3$ and $SrTiO_3$).[1] However, their epitaxial integration, already complex due to the dissimilar properties of the materials, is additionally complicated by the presence of the native silicon oxide.

Historically, the high-quality growth of materials on silicon was always preceded by the appropriate preparation of the silicon surface.[2−4] In fact, even now, after more than 40 years of development, approximately one-third of operations relate to wafer cleaning.[5] The commonly applied step in the process of silicon-surface decontamination and functionalization is a treatment with hydrofluoric acid that removes the layer of oxides and produces an H-terminated silicon surface.[6,7] However, the surface obtained in this manner is rough and faceted[8] with a tendency to reoxidize in ambient conditions.[9] One way to overcome this problem was to regrow, in controlled conditions, a layer of SiO_2 that can be removed by thermal desorption under ultra-high vacuum (UHV) conditions.[10]

Considering that flashing to 1150−1200 °C is limited to small samples that can be heated and cooled quickly,[11] a significant breakthrough in the deoxidation of silicon was achieved by applying a few monolayers of strontium or strontium oxide in a process initially developed for $SrTiO_3$ growth on a Si(100) surface.[12] Important findings that came from the approach were a notable reduction of the deoxidation temperature to 800 °C[12,13] and the formation of a strontium-covered surface that was less prone to oxidation.[14]

The interaction of alkaline-earth metals with a silicon surface has been studied in the past. Fan et al. investigated the adsorption of Sr and Ba on Si(001),[15,16] while in the pioneering works Ishiwara et al. investigated the epitaxial growth of $SrTiO_3$ on silicon using Sr/SrF_2 buffer layers.[17−19] However, an expansion of the research interest for the epitaxial growth of $SrTiO_3$ on a Si substrate occurred after McKee et al.'s work.[20] They showed that the heteroepitaxial growth of metal oxides

Received: August 4, 2014
Accepted: September 23, 2014
Published: September 23, 2014

 © 2014 American Chemical Society dx.doi.org/10.1021/am505202p | ACS Appl. Mater. Interfaces 2014, 6, 18205−18214

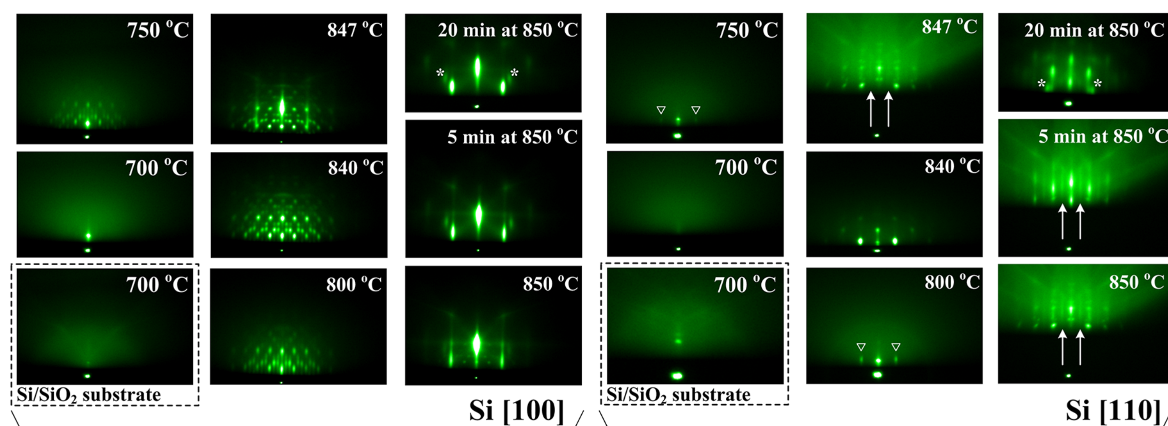

Figure 1. Characteristic sequences of the Si(001) surface deoxidation obtained using RHEED along the [100] and [110] azimuth of the Si(001) substrate. Please refer to the text for an explanation of the symbols.

requires the presence of a stable silicide template layer formed on the silicon surface.[20] From then on, strontium has been routinely used in molecular beam epitaxy (MBE) systems since it incorporates two advantageous features: native-oxide removal at lower temperatures and/or the formation of a silicide template layer.[13,21−27]

However, because of the high acquisition and operating costs, the low deposition rate, and the high reactivity of strontium, there is an interest in alternatives to MBE. For example, atomic layer deposition (ALD) was employed to prepare a strontium template on Si(100) by growing SrO using metal−organic surface reactions, followed by high-temperature annealing.[28,29] Motivated by the same reasons, we report on silicon surface deoxidation using a SrO thin film prepared using the pulsed-laser deposition technique (PLD). In the present study, reflection high-energy electron diffraction (RHEED), X-ray photoelectron spectroscopy (XPS), X-ray reflectivity (XRR), and atomic force microscopy (AFM) were used to analyze the SrO-induced deoxidation process at different annealing stages. To the best of our knowledge, this is the first report in which the useful features of alkaline-earth oxide and the PLD method were applied to silicon native-oxide removal.

■ EXPERIMENTAL DETAILS

The films were grown on 5 mm × 5 mm B-doped Si(100) substrates (Si-Mat, Germany). The substrates were ultrasonically cleaned in acetone for 3 min, thoroughly rinsed with EtOH, and blow-dried with a N_2 gun. Subsequently, the substrates were glued to a stainless-steel resistance heater using silver paste (Leitsilber 200, TedPella, Inc., USA). Prior to insertion into the PLD chamber (Twente Solid State Technology, Netherlands) the substrate was heated in the air (∼120 °C) to remove the organic solvent that is present in the paste. Once inserted into the PLD chamber, the substrates were degassed at 700 °C for 2 h.

After degassing, a KrF excimer laser (λ = 248 nm, 25 ns, COMPexPro 205 F, Coherent, Germany) was used for the (pre)ablation of the SrO single-crystalline target (SurfaceNet, Germany). During each deposition of the strontium oxide the fluency, repetition rate, spot size, and target-to-substrate distance were kept constant at 1.3 J/cm^2, 0.1 Hz, 2.31 mm^2, and 5.5 cm, respectively. The removal of the native oxide was studied by depositing 40 pulses of strontium oxide in a vacuum of ∼4 × 10^{-8} mbar on a Si/SiO_2 substrate at 700 °C, followed by an annealing stage. To determine the thickness of 40 pulses of SrO the two independent experiments were performed; that is, 1000 pulses of SrO were deposited on Si/SiO_2 in a vacuum of about 4 × 10^{-8} mbar at (i) room temperature and (ii) 700 °C, followed by deposition of thick protective TiO_2 layer (not shown). In both cases, the XRR analysis showed that thickness equivalent to 40 pulses is ∼0.86 nm, that is, ∼1.6 ML of SrO.

We selected different annealing temperatures, that is, 700, 750, 800, and 850 °C (for 20 min), while an additional sample was prepared at 200 °C as a control. The heating rate was 20 °C/min. Once the target temperature was reached, the sample was controllably cooled (20 °C/min) to 500 °C, after which the controlled cooling was turned off until a temperature of 200 °C was reached. Next, a protective TiO_2 layer (∼1.2 nm) was deposited (80 pulses, 1.3 J/cm^2, 1 Hz, 2.31 mm^2, 5.5 cm, 1.2 × 10^{-2} mbar Ar).

Both during the deposition of the SrO and the annealing, the surface of the sample was monitored *in situ* using the RHEED technique (RHEED gun with differential pumping, STAIB instruments, Germany, coupled with kSA 400 RHEED analysis system from k-Space Associates, Inc., USA). The chemical composition of the samples was obtained *ex situ* using an XPS system (Physical Electronics, Inc., USA) with a hemispherical analyzer and a multichannel detection system. Focused monochromatic Al radiation (1486.7 eV) was used as the photon source, while the spectrometer energy resolution was 0.3 eV. All the spectra were recorded at a takeoff angle of 80° (if not specified otherwise) and aligned with respect to the adventitious C 1s component at 284.8 eV. The surface composition was calculated from the XPS signals, taking into account the relative sensitivity factors provided by the manufacturer of the XPS spectrometer.[30] The surface composition of the layered structure present in our samples was calculated using a simplified model of a homogeneous matrix. The relative error of concentration determination by XPS was estimated to be ∼5%. For the purpose of qualitative analysis the XPS signals were deconvoluted using the FitXPS program from David Adams, University of Aarhus, Denmark. Immediately after the XPS analysis, the thickness of the films was analyzed *ex situ* using the XRR method (Empyrean with PIXCel^{3D} detector, PanAnalytical, Netherlands). The configuration on the incident side consisted of a programmable divergence slit with a 1/32° fixed divergence slit and a 1/16° fixed antiscatter slit, a fixed incident beam mask of 5 mm, and a 0.04 rad Soller slit. On the diffracted side a 0.27° parallel-plate collimator was used with the corresponding slit, a 0.04 rad Soller slit and a PIXCel^{3D} detector in the receiving-slit mode (all channels active). The XRR spectra were acquired in the ω-2θ mode in the range from 0.1° to 5° with a 0.005° step size and 11 s per step. The simulation of obtained curves was performed using dedicated X'Pert Reflectivity software and a segmented fit procedure, while taking into account the sample size (5 mm × 5 mm) and the beam width (0.075 mm). The same software package was used for error analysis. The surface morphology of the sample was examined using atomic force microscopy in the tapping mode (Veeco Dimension 3100 AFM/MFM system), while the images were processed using WSxM software.[31] The root-mean-square (RMS) value and relative error were obtained after measurement on three different places on the sample surface.

RESULTS AND DISCUSSION

Reflection High-Energy Electron Diffraction (RHEED). Figure 1 shows the characteristic sequences of the silicon surface deoxidation, at different stages of annealing, induced by a thin layer of strontium oxide. The azimuth directions of the Si(001) substrate are shown at the bottom of each segment containing a set of 3 × 3 RHEED images (Figure 1). The dashed rectangles indicate the RHEED images of the Si/SiO_2 substrate before the deposition, while the rest of the RHEED images in Figure 1 correspond to sample surface after the SrO deposition and subsequent annealing. On the basis of the diffuse patterns it is clear that both before and after the deposition of the SrO an amorphous layer is present on the silicon surface (700 °C, Figure 1). In the case of pristine silicon this is a consequence of the native oxide remaining after the degassing, while the latter is due to the amorphous nature of the deposited film.

The annealing of the deposited film induced a gradual change in the surface crystallinity, as evidenced by the appearance of bright spots (750 °C, [100] direction, Figure 1). Note that the transformation of the amorphous surface to an ordered one was observed during heating with a relatively fast rate (20 °C/min). This ramp rate was adopted to avoid substantial loss of SrO, since it is known that the desorption of the SrO peaks already at 550 °C.[29] The corresponding spots, observed along the [110] direction, were less pronounced, because of which the reversed triangles were used to indicate them (Figure 1, 750 °C). The definition of the spots, as well as the 3D character of the RHEED patterns, was improved with the annealing (up to 840 °C, Figure 1). Because of the intense bright spots along the [100] direction and the increased three-dimensional (3D) character of the RHEED patterns (from 750 to 840 °C), we refer to this structure as "3D" and the corresponding RHEED patterns as "spotty".

The observed "spotty" pattern was stable over a range of ~100 °C. At ~850 °C the formation of 1× streaks (847 °C, [100] direction, Figure 1) and 2× streaks (847 °C, arrows, [110] direction, Figure 1) became apparent. The intensity of the streaks increased with the temperature, and at 850 °C the streaks were clearly visible (Figure 1). The observation of 1× and 2× streaks suggests that the 2 × 1 Sr-induced reconstruction of the silicon surface was achieved. Clearly, the 3D structure and the 2 × 1 reconstructed surface coexist (847−850 °C, Figure 1). After 5 min at 850 °C only the 2 × 1 Sr-reconstructed surface remains. Also, prolonged annealing at 850 °C led to the loss of definition of the half-order streaks, while the definition of the spots corresponding to the SiC, due to imperfect vacuum, was improved (marked with * in Figure 1). The discussion about the possible origin of the 3D structure is given after the introduction to the XPS and XRR data.

X-ray Photoelectron Spectroscopy. The XPS analysis was performed after a batch of samples was prepared. Because of the transfer of the samples to the XPS UHV chamber their surface was exposed to air for about 15 min. On the basis of the quantitative information from the XPS analysis, obtained using a model of a homogeneous matrix, we were able to assess the concentration profiles of the silicon surface after different stages of annealing. The atomic concentrations of the O, Ti, Sr, and Si are shown in Figure 2. The concentration of carbon is not presented, although its contribution in total atomic concentration was accounted for. Clearly, the concentration of Ti and O is constant for all samples, which can be ascribed to the TiO_2 capping layer, while the concentration of Sr decreases (Figure 2). The decrease of the Sr concentration was enhanced at temperatures higher than 700 °C due to desorption and deoxidation processes occurring on the surface, which can explain the increase of the Si concentration (Figure 2).

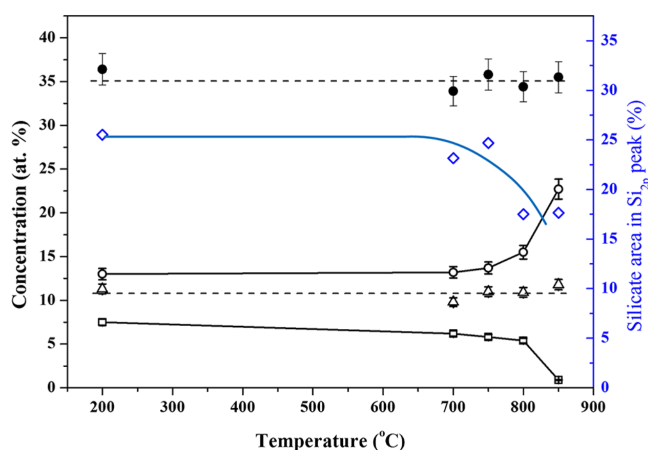

Figure 2. Atomic concentrations of O (-●-), Ti (-Δ-), Sr (-□-), and Si (-○-) and the amount of silicate in the Si 2p peak (-◇-) obtained by XPS (right *y*-axis).

The normalized core-level spectra reveal the chemical state of the annealed samples (Figure 3). The positions of Ti $2p_{1/2}$ and Ti $2p_{3/2}$ at 464.3 and 458.5 eV, respectively, and their separation of ~5.8 eV is an apparent characteristic of the TiO_2 (Figure 3a).[32−34] The C 1s core-level spectra of the prepared samples are shown in Figure 3b. The intense peak at 284.8 eV can be ascribed to C−C bonds as a result of the carbon contamination present on the sample surface. On the side of the lower binding energies, another peak can be observed at 279.3 eV. This peak is clearly visible for samples annealed up to 800 °C, while it disappears in the case of the sample annealed for 20 min at 850 °C (Figure 3b). Similar behavior was observed in the case of the doublet positioned at 135.0 and 133.2 eV (850 °C, Figure 3d, please note the signal-to-noise ratio). The peaks observed at 279.3, 135.0, and 133.2 eV correspond to Sr $3p_{1/2}$, Sr $3d_{3/2}$, and Sr $3d_{5/2}$, respectively, and provide evidence for the $SrCO_3$.[35,36] The deconvoluted Sr 3d spectra of the sample prepared at 200 °C indicate the presence of a single Sr-containing component, that is, $SrCO_3$ (Figure 4a). This indicates insufficient capping of the TiO_2 protective layer, because of which the reaction of the SrO with CO_2 from the air occurred (by forming $SrCO_3$).

The Si 2p spectra are shown in Figure 3e. The doublet at ~98.9 eV and the broad peak at 103.0 eV, observed in the case of the pristine, ultrasonically cleaned, silicon substrate, are characteristic for Si and SiO_2, respectively. However, in the case of all the annealed samples the peak at 103.0 eV was shifted to lower binding energies (101.3−101.7 eV), which suggests the formation of silicates.[37−41] By deconvoluting the Si 2p spectra (Figure 4b), the contribution of the silicate peak to the total Si 2p signal can be used for assessing the temperature evolution of the amount of silicate (Figure 2, right axis). The results show a decrease in the amount of silicate after the high-temperature treatments, which is in line with the temperature trends of the atomic concentration of strontium (Figure 2). Therefore, on the basis of the XPS data, the components of the multilayer of thin films can be identified as TiO_2, $SrCO_3$, Sr-silicate, and Si as a substrate. Figure 3c shows the O 1s spectra of the initial Si/

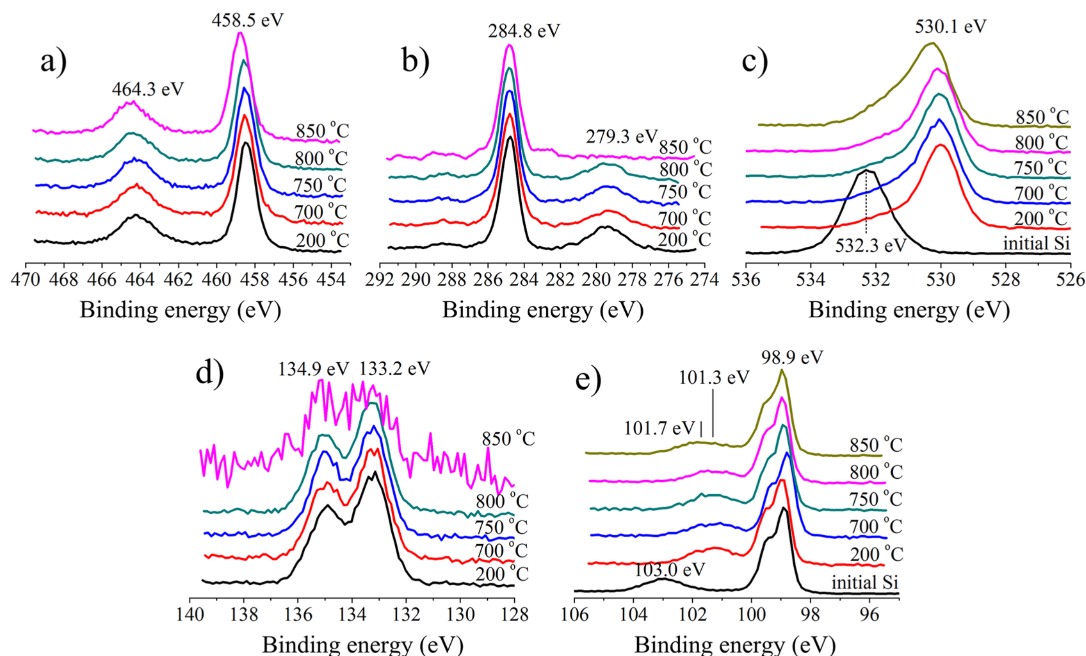

Figure 3. Normalized core-level spectra of (a) Ti 2p, (b) C 1s, Sr $3p_{1/2}$ (c) O 1s, (d) Sr 3d, and (e) Si 2p of the samples annealed at different temperatures.

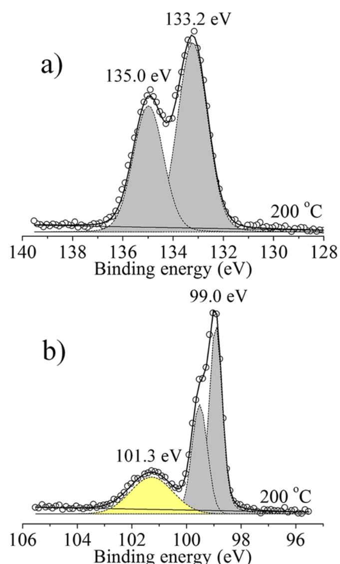

Figure 4. Deconvoluted (a) Sr 3d and (b) Si 2p core-level spectra of the sample prepared at 200 °C.

SiO_2 and annealed samples. Clearly, the O 1s spectra of the annealed samples are convoluted due to the contributions of the TiO_2, $SrCO_3$, and Sr-silicate. A further discussion of the XPS results, in particular those of O 1s, is presented after the introduction of the XRR results.

X-ray Reflectometry. The XRR curves were recorded immediately after the XPS analysis. The samples were stored in a glovebox with a controlled inert atmosphere before they were measured in the air using the XRR method. The obtained XRR curves are shown in Figure 5. To obtain the information about the film thickness the fitting of experimental curves was based on components identified by XPS (TiO_2, $SrCO_3$, Sr-silicate, and Si). Since the deposition of the TiO_2 capping layer was performed under the same conditions for all the samples, only a small variation of the TiO_2 thickness should be expected. To determine the thickness of the TiO_2 capping layer, an additional experiment (not shown) involving 1000 pulses of

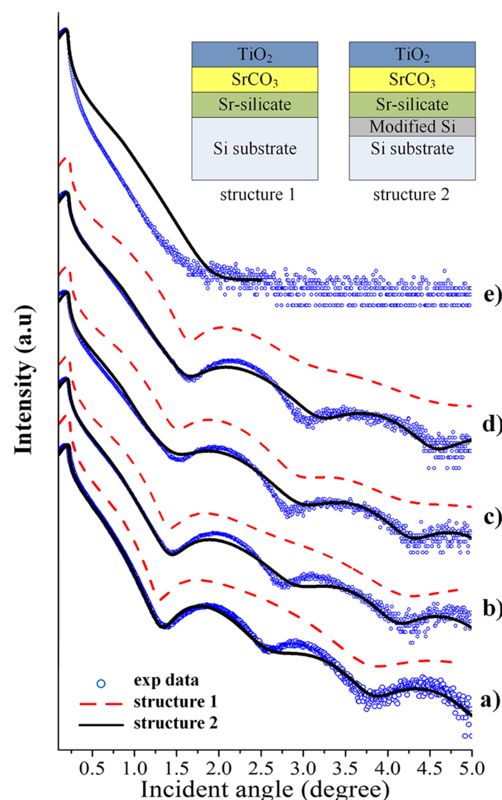

Figure 5. X-ray reflectivity curves of samples annealed at (b) 700 °C, (c) 750 °C, (d) 800 °C, and (e) 850 °C for 20 min, with a control sample prepared at 200 °C (a). (inset) Two multilayer structures used for the fitting of the XRR data. The Sr-silicate compound is Sr_2SiO_4 in (a) and $SrSiO_3$ in (b−e). Please note that the fitting curve corresponding to structure 1 has an offset for clarity.

TiO_2 deposited on a Si/SiO_2 substrate was conducted under the same conditions as in the case of the annealed samples. The results showed, assuming a constant growth per pulse in the applied pulse range, that the thickness of 80 pulses of TiO_2 used for capping the annealed samples is 1.23 nm.

While the identification of the TiO_2, $SrCO_3$, and Si from the XPS data was straightforward, the case with the silicate component was more complex. The reported binding energies of the Sr-silicate (usually described as $Sr_xSi_yO_z$) in the Si 2p core-level spectra range from 101.5 to 103.1 eV, where the majority of the data are centered around 102.2 eV.[14,38−44] Some authors ascribed this binding energy (102.2 eV) to Sr_2SiO_4.[38−40] The silicate peak in our case is between 101.3 and 101.7 eV (Figure 3e), because of which it was difficult to state the exact stoichiometry. However, it was reported that Sr_2SiO_4 tends to transform to $SrSiO_3$ when annealed above 600 °C.[39] Since in our case the samples were annealed above 700 °C, we believe that the temperature transformation of the silicate occurred, because of which we implemented $SrSiO_3$ as a strontium silicate component. In the case of sample prepared at 200 °C the silicate was approximated by Sr_2SiO_4.

Therefore, a multilayer structure, composed of TiO_2, $SrCO_3$, Sr-silicate, and the Si substrate, was initially proposed (structure 1, Figure 5). The restrictions imposed on the multilayer structure during the simulation of the XRR curves were (i) the density variation of each component is not higher than 10%, (ii) the thickness of the TiO_2 capping should be 1.23 nm (±10%), and (iii) the roughness of the film cannot be greater than the film thickness. The obtained curves show that the position of the critical angle and the first fringe is well-matched, while at higher angles (>1.75°) there is a discrepancy, since the simulated curves do not adequately describe the presence of fringes (dashed lines in Figure 5).

As pointed out by Dane et al.,[45] there are several factors that can complicate the analysis of the data: (i) different sample compositions for which the reflectivity curves are more or less the same, (ii) multiple runs until a feasible sample composition and good fits were obtained, (iii) the user has to decide whether or not the solution obtained is feasible, and (iv) the addition of extra interfacial layers to a multilayer structure of thin film. In the case when knowledge about the thin film is scarce it is clear that obtaining valid information can be time-consuming. One way to improve the matching, as pointed out by Dane et al.,[45] is to introduce a new component to the multilayer structure. However, in our case, the selection of additional components is limited by the XPS results, which include only TiO_2, $SrCO_3$, Sr-silicate, and Si as the substrate.

It is known that the PLD method produces energetic species with energies up to a few kiloelectron volts, because of which it is also considered for a unique hyperthermal deposition technique.[46] This is a consequence of energy transfer from UV-laser pulse to kinetic energy of the particles in the plum. In the absence of gases to slow down the plume there is a wide range of particle−solid interactions that can occur. The observation of a silicate peak in the Si 2p spectra of the sample prepared at 200 °C supports such reasoning (Figure 4b). Namely, in numerous MBE experiments the formation of silicate from strontium oxide was observed at temperatures above 400 °C.[39,40,42] In our experiments, the silicate was obtained for a sample prepared already at 200 °C (-◇-, Figure 2 and Figure 4b) and therefore, since the SrO was deposited in a vacuum, the formation of silicate at low temperatures can be explained by the interaction between the SrO plume and the Si/SiO_2 substrate, as a consequence of the ballistic implantation and mixing.[46] At the same time, the energetic particles of the plume can enhance the atomic mobility, amorphization, and collisional cascades, because of which the topmost layer of the Si substrate can be changed.

According to this, we have added modified silicon as an additional layer to the previously proposed structure (structure 2, Figure 5). This required a new restriction to be added; that is, the change in the density of the Si substrate must be excluded, while the other conditions were unchanged. As can be observed from Figure 5, the matching of the simulated curves with experimental data was significantly improved: the position of the critical angle and fringes is well-described, while the discrepancy between the experimental and simulated curves was considerably reduced (solid lines in Figure 5).

The thickness of the modified silicon layer and the thickness of the strontium-containing layers, as a sum of the Sr-silicate (Sr_2SiO_4 at 200 °C and $SrSiO_3$ at $T \geq 700$ °C) and $SrCO_3$ thickness, together with the total thickness, are given in Figure 6. The thicknesses were obtained after fitting the XRR data

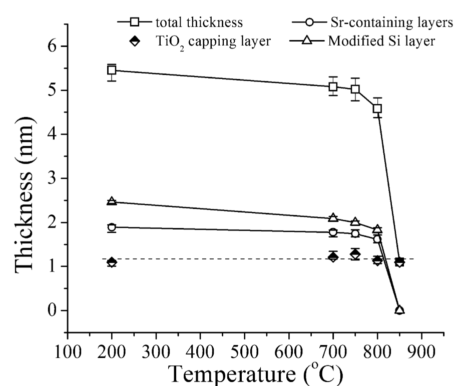

Figure 6. Variation of film thickness with temperature.

based on structure 2 (Figure 5). Clearly, the TiO_2 thickness is constant due to consistent capping, while the total thickness of the film starts to decrease above 700 °C. Similar trends were observed in the case of strontium-containing layers and the modified Si layer (Figure 6). The decrease in the total thickness is a result of desorption and deoxidation of the SrO/silicates at higher temperatures, while the decrease of the modified Si-layer thickness agrees well with the expected defect annealing at high temperatures. By comparing the temperature changes of the atomic concentration (Figure 2) and the film thickness (Figure 6) it is clear that the trends are similar. Also, the increasing trend of Si concentration in Figure 2 is in line with the XRR data and can be justified by an increase in the sampling volume of the Si substrate as the film thickness is decreased. Similar trends for the Si 2p (substrate), Si 2p (silicate), and Sr 3d peak intensities as a function of the annealing temperature were observed in the Muller-Sajak et al. study.[40]

The change in roughness of each layer, obtained by fitting the XRR results, is shown in Figure 8a. The roughness of the Sr-silicate and the Si substrate is almost constant up to 800 °C, while the roughnesses of the $SrCO_3$ and the modified Si layer increase slightly with temperature. The constant roughness of the Si substrate is a consequence of the model structure, since all changes in the Si substrate are reflected in changes to the modified Si layer. After 20 min of annealing at 850 °C the thicknesses of the Sr-containing layers decrease to zero (Figure

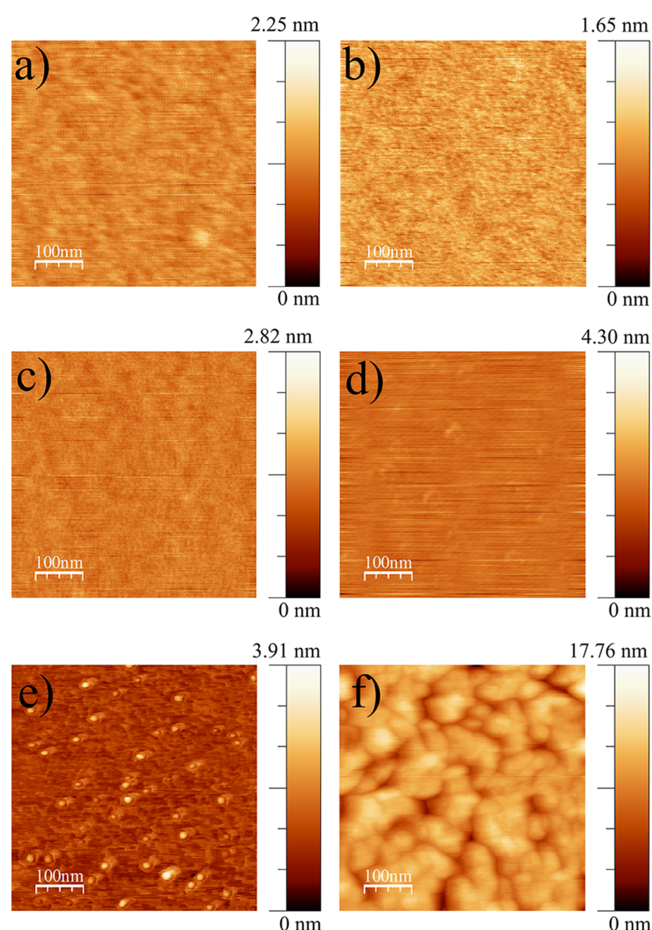

Figure 7. AFM micrographs of (a) initial Si/SiO_2 substrate and samples annealed at (b) 200 °C, (c) 700 °C, (d) 750 °C, (e) 800 °C, and (f) 850 °C for 20 min.

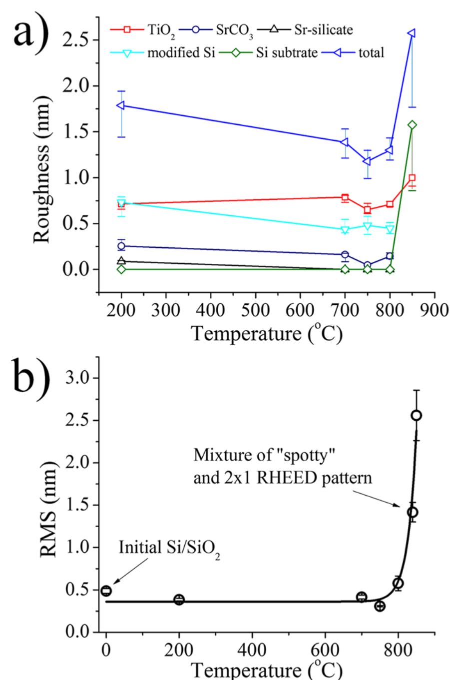

Figure 8. Roughness of samples annealed at different temperatures, as obtained using the (a) XRR and the (b) AFM method. RMS values were obtained from an area of 100 μm^2.

6 and the signal-to-noise ratio of the Sr 3d peak in Figure 3d), because of which the presentation of the roughness of $SrSiO_3$ and $SrCO_3$ at 850 °C has no physical meaning. The same is true for the modified Si layer. Finally, it can be observed that TiO_2 provides the dominant contribution to the overall roughness up to 800 °C. However, at 850 °C, after prolonged annealing, the roughness of the Si substrate becomes dominant. By assuming the cumulative nature of the roughness of each component, the total roughness, as a sum of roughness of each component, can be obtained (Figure 8a). The results of the XRR method were compared with the results of the atomic force microscopy.

Atomic Force Microscopy. The AFM analysis showed that the morphology (Figure 7) and roughness of the sample surfaces (Figure 8b) change with annealing. In the case of the samples annealed up to 750 °C the average roughness remained similar to the initial Si/SiO_2 substrate (Figure 7a–d and Figure 8b). In the case of the sample annealed to 800 °C the formation of circular protrusions was observed (Figure 7e), but after prolonged annealing at 850 °C they disappeared, leaving the surface with a drastically increased roughness (Figure 7f). By comparing the total roughness obtained using the XRR method (Figure 8a) with the RMS values of the AFM method (Figure 8b), the matching of the trend is clearly visible. We also prepared a sample showing a mixture of 2 × 1 and the "spotty" RHEED pattern, and the roughness of such a surface agrees well with the trend of the RMS increase (Figure 8b). Having in mind the decrease in the thickness of the Sr-containing layers with temperature (Figure 6), the increase in the roughness, as observed using the AFM and XRR methods (Figure 8), can be explained by Wei et al.'s finding that an insufficient amount of SrO promotes the formation of a rough silicon surface during the deoxidation process.[13]

Analysis of 3D Structure. To identify the origin of the 3D structure (Figure 1, 750–850 °C), we prepared an additional set of samples (Table 1). Although the previous XPS results clearly indicated the presence of TiO_2, $SrCO_3$, and Sr-silicate (Figure 3), the contribution of each component to the O 1s is less straightforward because they overlap. Therefore, special attention was devoted to the O 1s peak, which is, in our opinion, important for understanding the origin of the 3D structure.

Table 1. Preparation and Growth Conditions for Samples without a TiO_2 Protective Layer

sample	preparation[a]
S0	5 × 5 mm Si/SiO_2 substrate is ultrasonically cleaned in acetone for 3 min, rinsed with EtOH, and blow-dried with a N_2 gun[b]
S1	Initial cleaning + 80 pulses of TiO_2 at 0.03 mbar O_2 at T_{room} + exposure to air for 15 min
S2	Initial cleaning + 40 pulses of SrO at 0.2 mbar O_2 at T_{room} + exposure to air overnight
S3	Initial cleaning +2 h of degassing at 700 °C + 1h cooling +40 pulses of SrO at $\sim 4 \times 10^{-8}$ mbar at $T < 100$ °C + exposure to air[c]
S4	Initial cleaning + 2 h of degassing at 700 °C + 40 pulses of SrO at $\sim 4 \times 10^{-8}$ mbar at $T = 700$ °C + heating until a sharp "spotty" RHEED pattern was observed + exposure to air[c]

[a]The fluency, repetition rate, spot size, and target-to-substrate distance during the deposition of the SrO and TiO_2 were the same as in the previous set of experiments. [b]Referred to as initial cleaning. [c]The samples were allowed to cool to room temperature in the PLD chamber before they were exposed to air for 15 min prior to XPS measurements.

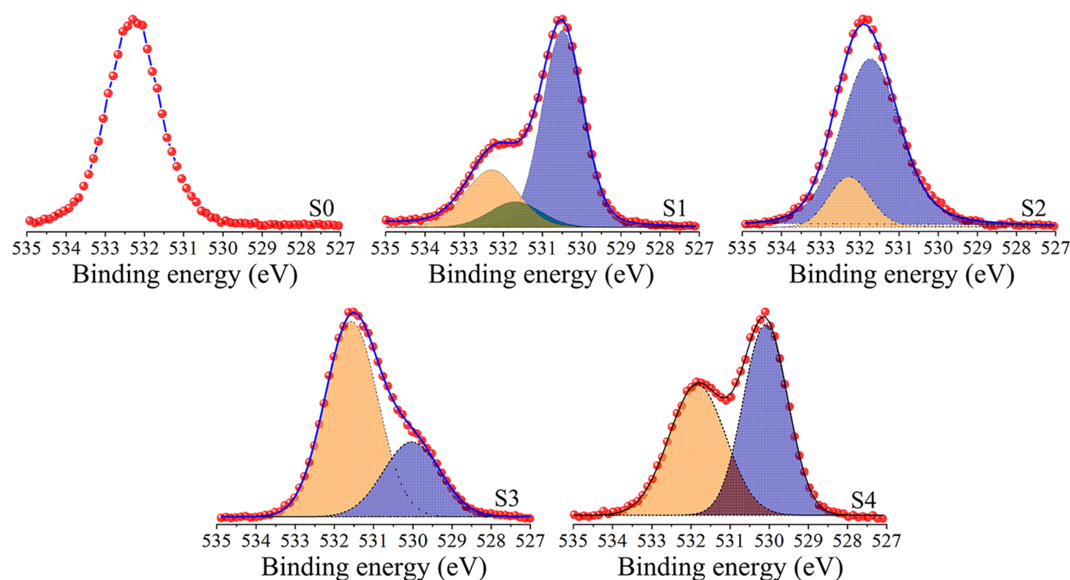

Figure 9. O 1s core-level spectra of samples described in Table 1.

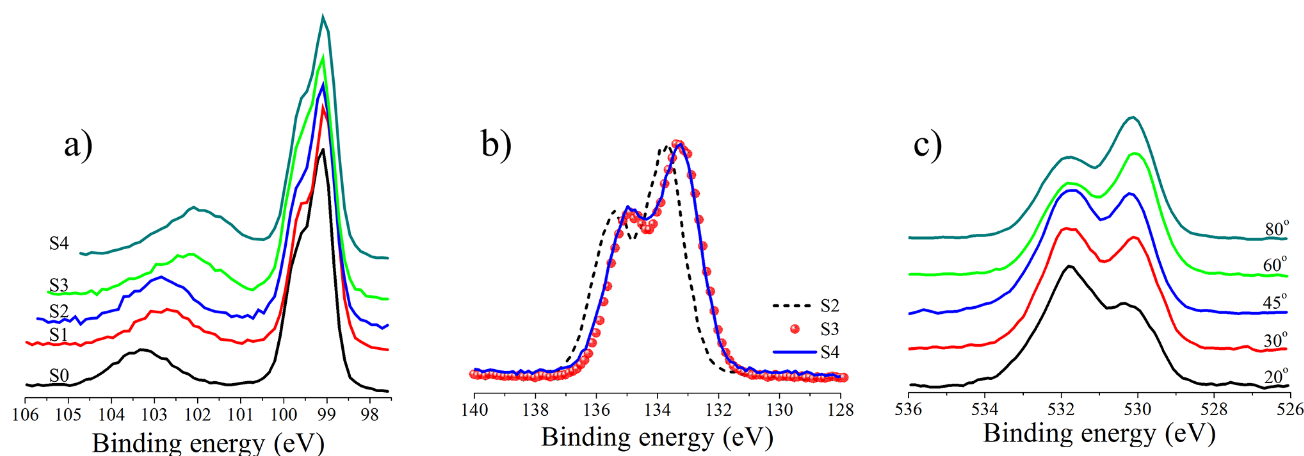

Figure 10. Normalized (a) Si 2p and (b) Sr 3d core-level spectra of the samples S0−S4 described in Table 1 (takeoff angle is 80°). (c) The angle-resolved O 1s spectra of sample S4.

In a new set of experiments the SrO films were prepared without a TiO_2 protective layer. As was shown previously, a 1.2 nm thick layer of TiO_2 was not sufficient to prevent the interaction of the SrO with CO_2 from the air (i.e., the formation of carbonates, Figure 3d). It is important to note that we prepared thicker TiO_2 films (∼20 nm) that efficiently prevented any interaction with the air; however, in such cases it is necessary to probe the corresponding interface using XPS in combination with ion-beam sputtering. Unfortunately, the interface appeared as "blurred" due to the ion-beam mixing induced by the Ar ions. Therefore, we intentionally prepared samples without a protective layer, aware of the unavoidable interaction of the film with the air under ambient conditions. To slow down the particles in the plume, in a new set of experiments the deposition of TiO_2 and SrO was performed in 0.03 mbar and 0.2 mbar of O_2, respectively. The process pressure during the deposition of the TiO_2 and the SrO was selected to understand the role of the pressure, that is, the particle energy, on the formation of the initial multilayer structure.

The O 1s core-level spectra of the samples S0, S1, and S2 that act as a reference for the SiO_2, TiO_2, and $SrCO_3$, respectively, are shown in Figure 9. The O 1s spectrum of the sample S1 can be deconvoluted into three peaks centered at 530.5 eV (TiO_2),[47] 531.7 eV (OH groups on TiO_2),[48] and 532.3 eV (SiO_2). Similarly, the O 1s peak of the sample S2 can be deconvoluted into two components: one belonging to SiO_2 (532.3 eV) and the other at 531.7 eV that can be ascribed to $SrCO_3$, due to overnight exposure of the SrO film to the air. The O 1s spectra of the samples S3 and S4 can be deconvoluted with two components centered at 531.6 and 530.0 eV and 531.8 and 530.1 eV, respectively (Figure 9). Clearly, the peak at ∼531.7 of the samples S3 and S4 is well-matched to the one of the $SrCO_3$ (sample S2). Also, the Sr 3d peak of the samples S2−S4 (Figure 9b) was observed at approximately the same binding energy (given the energy resolution) as in the first set of experiments (Figure 3d). This indicates that the Sr 3d spectra in Figure 3d contain information not only from the $SrCO_3$ but also from the Sr-silicate. To understand the origin of the O 1s peak at ∼530.1 eV it is necessary to explain the changes in the Si 2p core-level spectra (Figure 10a).

The doublet of the Si 2p core-level spectra of the S1−S4 samples was aligned with the Si $2p_{3/2}$ peak of the semi-

conducting silicon of the initial Si/SiO_2 substrate, S0 (Figure 10a). The binding energy difference of ∼4.3 eV between the doublet and the broad peak at 103.2 eV of sample S0 is characteristic of the Si/SiO_2 surface. On the other hand, for the S1−S4 samples the broad peak at 103.2 eV was shifted to the low-binding-energy side: S1 (102.7 eV), S2 (102.8 eV), S3 (102.3 eV), and S4 (102.0 eV). The shift to the low-binding-energy side was more pronounced if the films were deposited in a vacuum (S3 and S4, 4×10^{-8} mbar). In the case of samples S1 and S2, deposited at 0.03 mbar and 0.2 mbar, the shift toward lower binding energies was 0.5 and 0.4 eV, respectively, while in the case of samples S3 and S4 it was 1.0 and 1.3 eV. This downward shift of the broad peak is attributable to the increase of the films' "silicate" character, that is, to the incorporation of a heteroatom in the SiO_2 matrix.[49]

In our opinion, the O 1s peak at 530.1 eV observed in the case of the S3 and S4 samples (Figure 9) can be ascribed to the layer with an increased "silicate" nature, induced by the ballistic implantation and the mixing of SrO with the silicon native oxide due to the deposition in a vacuum, while in the case of sample S4 the increased intensity of the peak at 530.1 eV can be ascribed to the contribution of the thermal treatment that was necessary for the appearance of a spotty RHEED pattern, that is, a 3D structure.

The origin of the O 1s peak at 530.1 eV (Figure 9, S3 and S4) can be found in the analogy with silicate glasses. One of the many methods used for the preparation of silicate glasses is ion implantation[50,51] and the quenching of silicate melts.[52,53] For example, in Dalby et al.'s study the silicate glass was obtained by the rapid cooling of $PbO-SiO_2$ melts in a liquid-nitrogen-cooled steel mold.[53] The analysis of the $PbO-SiO_2$ glass system revealed two O 1s peaks: one, the high-binding-energy O 1s peak representing the bridging oxygen (BO, originating from Si−O−Si) and the second, the lower-energy peak, representing both the nonbridging oxygen (NBO, originating from the Si−O−Pb) and the metal-bridging oxygen (MBO, originating from the Pb−O−Pb) contributions.[53] The same notation was used in Kakushima et al.'s study for the description of the La_2O_3 reaction with a HF-etched silicon surface, where the formation of the NBO Si−O−La peak was explained as being a consequence of the La_2O_3 reaction with Si diffused from the bulk.[54] Similarly, in Qin et al.'s study the observation of the O 1s peak at ∼529.7 eV was attributed to the formation of manganese silicate as a result of the MnO reaction with SiO_2 at elevated temperatures.[55]

Because of the deposition in a vacuum and the subsequent annealing, we believe that the peak at 530.1 eV can be ascribed to the Si−O−Sr type of bonds (NBO). This is corroborated by the Si 2p core-level spectra, where a clear downward shift was observed (Figure 10a). By analogy with the silicate glass, the O 1s spectra of samples S3 and S4 might reveal, in addition to the silicate phase, the features of different chemical environments present in the SiO_2 (BO) and SrO (MBO). For example, as sample S2 shows, the O 1s spectrum of the SiO_2 is overlapped by the O 1s spectrum of the $SrCO_3$ (Figure 9). However, because of that the identification of the SiO_2 is hindered in the S3 and S4 samples. Also, since the NBO (silicate) and MBO (SrO) contribute to the same peak,[53] it should be expected that the O 1s spectra of the SrO also contributes to the peak at 530.1 eV (Figure 9, S3 and S4). Indeed, numerous studies focused on the strontium−silicon interaction reported, although with some dissipation, that the position of the O 1s peak of the Sr−O bond is centered at ∼530.1 eV.[14,23,35,39,40,42−44,56,57] In our case, because of exposure to the air, the remaining SrO reacted to form $SrCO_3$, so the contribution to the peak at 530.1 eV (Figure 9, S3 and S4) is absent.

We further performed an angle-resolved XPS study of the sample S4, which provides a better insight into the ordering of layers. As is clear from Figure 10c the intensity of the NBO peak at ∼530.1 eV increases as the takeoff angle changes from 20° to 80°. This clearly shows that the silicate layer is under the layer of SrO, that is, the $SrCO_3$ formed after exposure to the air. In the present work, the exclusion of TiO_2 as a capping layer was proven to be very useful for a description of the process since the O 1s component of the TiO_2 and OH-groups on TiO_2 was overlapping the NBO peak of the formed silicate as well as the O 1s spectra of the $SrCO_3$, respectively.

CONCLUSION

On the basis of the obtained results the overall process of silicon native-oxide removal can be described in the following way. The deposition of SrO in a vacuum leads to the implantation of high-energy particles of the plume into Si/SiO_2, which results in the formation of the silicate layer, even at low temperatures (200 °C) and, possibly, the modification of the silicon substrate, while the low-energy part of the plume remains on the surface as SrO. Subsequent annealing promotes the desorption of the as-formed layers and deoxidation of the surface at sufficiently high temperatures. During this process, as observed by RHEED, the surface ordering occurs. On the basis of AFM and the 3D character of the RHEED patterns, this ordering leads to the formation of epitaxial, presumably SrO, islands and a 2 × 1 Sr-reconstructed silicon surface. However, the stability of the reconstructed surface is limited due to the increase of roughness and the formation of SiC.

The results indicate the necessity for optimizing the experimental conditions so a suitable quality of Sr-reconstructed surface is achieved. In our opinion, such an improvement would be a major milestone in the application of the PLD method for the integration of functional oxides with silicon.

AUTHOR INFORMATION

Corresponding Author

*E-mail: zjovanovic@vinca.rs. Phone: +381 11 6447700. Fax: +381 11 6447963.

Notes

The authors declare no competing financial interest.

ACKNOWLEDGMENTS

The research was financially supported by the Slovenian Research Agency (Project No. J2-6759).

REFERENCES

(1) Schlom, D. G.; Mannhart, J. Oxide Electronics: Interface Takes Charge Over Si. *Nat. Mater.* **2011**, *10*, 168−169.

(2) Kern, W. The Evolution of Silicon Wafer Cleaning Technology. *J. Electrochem. Soc.* **1990**, *137*, 1887−1892.

(3) Miki, K.; Sakamoto, K.; Sakamoto, T. Surface Preparation of Si Substrates for Epitaxial Growth. *Surf. Sci.* **1998**, *406*, 312−327.

(4) Heyns, M. M.; Nemanich, R. J. Wet Chemical Cleaning and Surface Preparation of Si. In *Properties of Crystalline Silicon;* Hull, R., Ed.; INSPEC: London, U.K., 1999; Vol. *20*, pp 219−225.

(5) Ruzyllo, J. Semiconductor Cleaning Technology: Forty Years in the Making. *Electrochem. Soc. Interface* **2010**, *19*, 44−46.

(6) Takahagi, T.; Nagai, I.; Ishitani, A.; Kuroda, H.; Nagasawa, Y. The Formation of Hydrogen Passivated Silicon Single-Crystal Surfaces Using Ultraviolet Cleaning and HF Etching. *J. Appl. Phys.* **1988**, *64*, 3516−3521.

(7) Trucks, G. W.; Raghavachari, K.; Higashi, G. S.; Chabal, Y. J. Mechanism of HF Etching of Silicon Surfaces: A Theoretical Understanding of Hydrogen Passivation. *Phys. Rev. Lett.* **1990**, *65*, 504−507.

(8) Chabal, Y. J.; Higashi, G. S.; Raghavachari, K.; Burrows, V. A. Infrared Spectroscopy of Si(111) and Si(100) Surfaces After HF Treatment: Hydrogen Termination and Surface Morphology. *J. Vac. Sci. Technol., A* **1989**, *7*, 2104−2109.

(9) Zhang, X.; Garfunkel, E.; Chabal, Y. J.; Christman, S. B.; Chaban, E. E. Stability of HF-Etched Si(100) Surfaces in Oxygen Ambient. *Appl. Phys. Lett.* **2001**, *79*, 4051−4053.

(10) Ishizaka, A.; Shiraki, Y. Low Temperature Surface Cleaning of Silicon and Its Application to Silicon MBE. *J. Electrochem. Soc.* **1986**, *133*, 666−671.

(11) Wilk, G. D.; Wei, Y.; Edwards, H.; Wallace, R. M. In Situ Si Flux Cleaning Technique for Producing Atomically Flat Si(100) Surfaces at Low Temperature. *Appl. Phys. Lett.* **1997**, *70*, 2288−2290.

(12) Yu, Z.; Ramdani, J.; Curless, J. A.; Overgaard, C. D.; Finder, J. M.; Droopad, R.; Eisenbeiser, K. W.; Hallmark, J. A.; Ooms, W. J.; Kaushik, V. S. Epitaxial Oxide Thin Films on Si(001). *J. Vac. Sci. Technol., B* **2000**, *18*, 2139−2145.

(13) Wei, Y.; Hu, X.; Liang, Y.; Jordan, D. C.; Craigo, B.; Droopad, R.; Yu, Z.; Demkov, A.; Edwards, J. J. L.; Ooms, W. J. Mechanism of Cleaning Si(100) Surface Using Sr or SrO for the Growth of Crystalline $SrTiO_3$ Films. *J. Vac. Sci. Technol., B* **2002**, *20*, 1402−1405.

(14) Liang, Y.; Gan, S.; Engelhard, M. First Step Towards the Growth of Single-Crystal Oxides on Si: Formation of a Two-Dimensional Crystalline Silicate on Si(001). *Appl. Phys. Lett.* **2001**, *79*, 3591−3593.

(15) Fan, W. C.; Wu, N. J.; Ignatiev, A. Observation of Ordered Structures of Sr on the Si(100) Surface. *Phys. Rev. B: Condens. Matter Mater. Phys.* **1990**, *42*, 1254−1257.

(16) Fan, W. C.; Ignatiev, A. Identification of Ordered Atomic Structures of Ba on the Si(100) Surface. *Surf. Sci.* **1991**, *253*, 297−302.

(17) Bum, Ki. M.; Hiroshi, I. Growth of Crystalline $SrTiO_3$ Films on Si Substrates Using Thin Fluoride Buffer Layers and Their Electrical Properties. *Jpn. J. Appl. Phys.* **1994**, *33*, 5911−5916.

(18) Hiroyuki, M.; Hiroshi, I. Epitaxial Growth of $SrTiO_3$ Films on Si(100) Substrates Using a Focused Electron Beam Evaporation Method. *Jpn. J. Appl. Phys.* **1991**, *30*, L1415−L1417.

(19) Bum, Ki. M.; Hiroshi, I. Roles of Buffer Layers in Epitaxial Growth of $SrTiO_3$ Films on Silicon Substrates. *Jpn. J. Appl. Phys.* **1994**, *33*, 1472−1477.

(20) McKee, R. A.; Walker, F. J.; Chisholm, M. F. Crystalline Oxides on Silicon: The First Five Monolayers. *Phys. Rev. Lett.* **1998**, *81*, 3014−3017.

(21) Lettieri, J.; Haeni, J. H.; Schlom, D. G. Critical Issues in the Heteroepitaxial Growth of Alkaline-Earth Oxides on Silicon. *J. Vac. Sci. Technol., A* **2002**, *20*, 1332−1340.

(22) Li, H.; Hu, X.; Wei, Y.; Yu, Z.; Zhang, X.; Droopad, R.; Demkov, A. A.; Edwards, J.; Moore, K.; Ooms, W.; Kulik, J.; Fejes, P. Two-Dimensional Growth of High-Quality Strontium Titanate Thin Films on Si. *J. Appl. Phys.* **2003**, *93*, 4521−4525.

(23) Zachariae, J.; Pfnür, H. Growth Conditions, Stoichiometry, and Electronic Structure of Lattice-Matched SrO/BaO Mixtures on Si(100). *Phys. Rev. B: Condens. Matter Mater. Phys.* **2005**, *72*, 075410.

(24) Norga, G. J.; Marchiori, C.; Guiller, A.; Locquet, J. P.; Rossel, C.; Siegwart, H.; Caimi, D.; Fompeyrine, J.; Conard, T. Phase of Reflection High-Energy Electron Diffraction Oscillations During (Ba,Sr)O Epitaxy on Si(100): A Marker of Sr Barrier Integrity. *Appl. Phys. Lett.* **2005**, *87*, 262905.

(25) Goncharova, L. V.; Starodub, D. G.; Garfunkel, E.; Gustafsson, T.; Vaithyanathan, V.; Lettieri, J.; Schlom, D. G. Interface Structure and Thermal Stability of Epitaxial $SrTiO_3$ Thin Films on Si (001). *J. Appl. Phys.* **2006**, *100*, 014912.

(26) Kourkoutis, L. F.; Hellberg, C. S.; Vaithyanathan, V.; Li, H.; Parker, M. K.; Andersen, K. E.; Schlom, D. G.; Muller, D. A. Imaging the Phase Separation in Atomically Thin Buried $SrTiO_3$ Layers by Electron Channeling. *Phys. Rev. Lett.* **2008**, *100*, 036101.

(27) Mi, S.-B.; Jia, C.-L.; Vaithyanathan, V.; Houben, L.; Schubert, J.; Schlom, D. G.; Urban, K. Atomic Structure of the Interface Between $SrTiO_3$ Thin Films and Si(001) Substrates. *Appl. Phys. Lett.* **2008**, *93*, 101913.

(28) Willis, B. G.; Mathew, A. Growth of Ordered SrO Layers on Si(100) Using Metal-Organic Surface Reactions. *J. Vac. Sci. Technol., A* **2008**, *26*, 83−89.

(29) Zhang, C. B.; Wielunski, L.; Willis, B. G. Formation of Strontium Template on Si(100) by Atomic Layer Deposition. *Appl. Surf. Sci.* **2011**, *257*, 4826−4830.

(30) Moulder, J. F.; Stickle, W. F.; Sobol, P. E.; Bomben, K. D. *Handbook of X-Ray Photoelectron Spectroscopy;* Chastain, F., King, R. C., Jr., Eds.; Physical Electronics USA, Inc.: Chanhassen, MN, 1995.

(31) Horcas, I.; Fernández, R.; Gómez-Rodríguez, J. M.; Colchero, J.; Gómez-Herrero, J.; Baro, A. M. WSxM: A Software for Scanning Probe Microscopy and a Tool for Nanotechnology. *Rev. Sci. Instrum.* **2007**, *78*, 013705.

(32) Bange, K.; Ottermann, C. R.; Anderson, O.; Jeschkowski, U.; Laube, M.; Feile, R. Investigations of TiO_2 Films Deposited by Different Techniques. *Thin Solid Films* **1991**, *197*, 279−285.

(33) Leprince-Wang, Y. Study of the Initial Stages of TiO_2 Growth on Si Wafers by XPS. *Surf. Coat. Technol.* **2002**, *150*, 257−262.

(34) Chen, S.-Z.; Zhang, P.-Y.; Zhu, W.-P.; Chen, L.; Xu, S.-M. Deactivation of TiO_2 Photocatalytic Films Loaded on Aluminium: XPS and AFM Analyses. *Appl. Surf. Sci.* **2006**, *252*, 7532−7538.

(35) Young, V.; Otagawa, T. XPS Studies on Strontium Compounds. *Appl. Surf. Sci. (1977−1985)* **1985**, *20*, 228−248.

(36) Sosulnikov, M. I.; Teterin, Y. A. XPS Study of Calcium, Strontium, Barium and Their Oxides. *Dokl. Akad. Nauk SSSR* **1991**, *317*, 418−421.

(37) Guittet, M. J.; Crocombette, J. P.; Gautier-Soyer, M. Bonding and XPS Chemical Shifts in $ZrSiO_4$ Versus SiO_2 and ZrO_2 - Charge Transfer and Electrostatic effects. *Phys. Rev. B: Condens. Matter Mater. Phys.* **2001**, *63*, 125117.

(38) Delhaye, G.; El Kazzi, M.; Gaillard, S.; Gendry, M.; Hollinger, G. Formation of Epitaxial Strontium Oxide and Silicate on Silicon (001). *J. Phys. IV* **2006**, *132*, 285−289.

(39) El Kazzi, M.; Delhaye, G.; Merckling, C.; Bergignat, E.; Robach, Y.; Grenet, G.; Hollinger, G. Epitaxial Growth of SrO on Si(001): Chemical and Thermal Stability. *J. Vac. Sci. Technol., A* **2007**, *25*, 1505−1511.

(40) Müller-Sajak, D.; Islam, S.; Pfnür, H.; Hofmann, K. R. Temperature Stability of Ultra-Thin Mixed BaSr-Oxide Layers and Their Transformation. *Nanotechnology* **2012**, *23*, 305202.

(41) Spreitzer, M.; Egoavil, R.; Verbeeck, J.; Blank, D. H. A.; Rijnders, G. Pulsed Laser Deposition of $SrTiO_3$ on a H-Terminated Si Substrate. *J. Mater. Chem. C* **2013**, *1*, 5216−5222.

(42) Kirsch, P. D.; Ekerdt, J. G. Interfacial Chemistry of the Sr/SiO_xN_y/Si(100) Nanostructure. *J. Vac. Sci. Technol., A* **2001**, *19*, 2222−2231.

(43) Mesarwi, A.; Fan, W. C.; Ignatiev, A. Oxidation of the Si(100) Surface Promoted by Sr Overlayer: An X-ray Photoemission Study. *J. Appl. Phys.* **1990**, *68*, 3609−3613.

(44) Kazzi, M. E.; Delhaye, G.; Gaillard, S.; Bergignat, E.; Hollinger, G. Two Dimensional Sr Silicate Grown on Si(001) Studied Using X-ray Photoelectron Spectroscopy. *J. Phys. IV* **2006**, *132*, 87−90.

(45) Dane, A. D.; Veldhuis, A.; Boer, D. K. G. d.; Leenaers, A. J. G.; Buydens, L. M. C. Application of Genetic Algorithms for Characterization of Thin Layered Materials by Glancing Incidence X-ray Reflectometry. *Phys. B (Amsterdam, Neth.)* **1998**, *253*, 254−268.

(46) Gorbunoff, A. Cross-Beam PLD: Metastable Film Structures from Intersecting Plumes. In *Pulsed Laser Deposition of Thin Films: Applications-Led Growth of Functional Materials;* Eason, R., Ed; John Wiley & Sons, Inc.: New Jersey, USA, 2007; p 131.

(47) Gallas, B.; Brunet-Bruneau, A.; Fisson, S.; Vuye, G.; Rivory, J. SiO_2-TiO_2 Interfaces Studied by Ellipsometry and X-ray Photoemission Spectroscopy. *J. Appl. Phys.* **2002**, *92*, 1922−1928.
(48) Lazarus, M. S.; Sham, T. K. X-ray Photoelectron Spectroscopy (XPS) Studies of Hydrogen Reduced Rutile (TiO_{2-x}) Surfaces. *Chem. Phys. Lett.* **1982**, *92*, 670−674.
(49) Giustino, F.; Bongiorno, A.; Pasquarello, A. Modeling of Si 2p Core-Level Shifts at $Si-(ZrO_2)_x(SiO_2)_{1-x}$ Interfaces. *Appl. Phys. Lett.* **2002**, *81*, 4233−4235.
(50) Cattaruzza, E. Quantum-Dot Composite Silicate Glasses Obtained by Ion Implantation. *Nucl. Instrum. Methods Phys. Res., Sect. B* **2000**, *169*, 141−155.
(51) Barison, S.; Battaglin, G.; Bertoncello, R.; Cattaruzza, E.; Mascolo, A.; Mazzoldi, P.; Ruzzi, M.; Trivillin, F. Composite Materials Obtained by Ion Irradiation: Mn Implantation in Silica Glass. *J. Mater. Chem.* **1999**, *9*, 2929−2933.
(52) Nesbitt, H. W.; Bancroft, G. M.; Henderson, G. S.; Ho, R.; Dalby, K. N.; Huang, Y.; Yan, Z. Bridging, Non-Bridging and Free (O^{2-}) Oxygen in Na_2O-SiO_2 Glasses: An X-ray Photoelectron Spectroscopic (XPS) and Nuclear Magnetic Resonance (NMR) study. *J. Non-Cryst. Solids* **2011**, *357*, 170−180.
(53) Dalby, K. N.; Nesbitt, H. W.; Zakaznova-Herzog, V. P.; King, P. L. Resolution of Bridging Oxygen Signals From O 1s Spectra of Silicate Glasses Using XPS: Implications for O and Si Speciation. *Geochim. Cosmochim. Acta* **2007**, *71*, 4297−4313.
(54) Kakushima, K.; Tachi, K.; Song, J.; Sato, S.; Nohira, H.; Ikenaga, E.; Ahmet, P.; Tsutsui, K.; Sugii, N.; Hattori, T.; Iwai, H. Comprehensive X-ray Photoelectron Spectroscopy Study on Compositional Gradient Lanthanum Silicate Film. *J. Appl. Phys.* **2009**, *106*, 124903.
(55) Qin, X.; Sun, H.; Zaera, F. Thermal Chemistry of $Mn_2(CO)_{10}$ During Deposition of Thin Manganese Films on Silicon Oxide and on Copper Surfaces. *J. Vac. Sci. Technol., A* **2012**, *30*, 01A112.
(56) Vasquez, R. P. X-ray Photoelectron Spectroscopy Study of Sr and Ba Compounds. *J. Electron Spectrosc. Relat. Phenom.* **1991**, *56*, 217−240.
(57) Van Doveren, H.; Verhoeven, J. A. T. H. XPS Spectra of Ca, Sr, Ba and Their Oxides. *J. Electron Spectrosc. Relat. Phenom.* **1980**, *21*, 265−273.